



Optical properties of manganese chiral single ring by glancing angle deposition technique

*Mahsa F. **

Islamic Azad University Meybod Branch, Meybod, Iran

Received 25 June 2015; Revised 6 Nov. 2015; Accepted 2 March 2016

Abstract

Embracing physical vapor deposition system, GLAD method defines the deposition angle, α , in terms of vapor flux and normal substrate. The substrate rotation angle, φ , defines the azimuthal substrate position relative to an arbitrary starting position. We have fabricated periodic nanostructure through utilizing GLAD to control the film deposition conditions over these arrays. Manganese chiral single ring nanostructure has been created using oblique angle deposition method in conjunction with rotation of normal surface substrate. Employing AFM measurement and J-Microvision software, we obtained structure morphology, the size of grains, surface physical roughness and surface void fraction. The optical spectra of the samples were obtained using a single beam spectrophotometer for the incident light of the surface normal. Moreover, it should be mentioned here that Fresnel formulas and experimental measurements of reflectance and absorption spectra could be applied to obtain the refractive index n and the absorption index k . Since Manganese chiral single ring of fabricated nanostructure with GLAD technique is porous, the plot of the refractive index that was observed as a function of the wavelength index aspect has lower values in comparison with homogeneous Manganese thin film associated with longer wavelengths. Therefore, we can control the refractive index of nanostructure with regard to the film density and porous. It is suggested that GLAD may offer an effective method to attain tailor able refractive index.

Keywords: Reflection, Transmission, Absorption, Refractive index, Manganese chiral single ring.

1. Introduction

Metallic nano-structures which depend on their size and geometrical shape have laid the ground for researchers to conduct researches in different fields of application such as biomedicine [1-4], antibacterial [5-8], and optics [9-10].

The Oblique Angle Deposition or Glancing Angle Deposition (OAD and GLAD) method together with rotation of substrate about the substrate surface normal is used to create sculptured nanostructures with pre-designed shapes and desired porosity that can alter different properties at these films.

*) Corresponding author. Email: mahsa.fakharpour@yahoo.com

Owing to the fact that nanostructures of noble metals (gold, silver, and copper) have the ability of exhibiting Localized Surface Plasmon Resonances [11], they have many applications, particularly in the field of Plasmonics [12-16]. Experimental and theoretical investigations have shown that when the number of corners or recesses in the morphology of nanostructure goes up, it can produce higher number of sites to create enhanced fields facilitating Surface Enhanced Raman Spectroscopy (SERS) detection [17].

In 1959, Yong and Kowal used physical vapour deposition to provide helical fluorite films using a rotating substrate as well as the creation of man-made helical structures. They have shown that these thin films could rotate the plan of polarization of normally incident light [18]. Later, Motohiro and Taga that used Oblique Angle Deposition method created the simple chevron films of metal oxides and researched their birefringence properties [19]. In addition, Robbie and Brett prepared the aligned three-dimensional sculptured thin films using a Glancing Angle Deposition (GLAD) technique and studied their optical activity. They have shown that a porous TiO_2 helical thin film would select reflection of circularly-polarized light. When the pitch height increased, the reflection band was subsequently shifted to longer wavelength [20-21].

Therefore, the optical properties of helical structures made from materials such as noble metals for example Ag and Au will be expected to be very different from those made from dielectrics [22]. After that, Zhang and Zhao in their paper studied the pitch height-dependent and the polarization angle-dependent optical properties of Ag helical nanostructures [23]. In the current study, we report optical properties such as reflection, transmittance, absorption, and also refractive and absorption indices of Manganese chiral single ring on the glass substrate that was prepared by GLAD method.

2. Experimental Details

Prior to being deposited, all glass substrates were ultrasonically cleaned in heated acetone before deposition then ethanol at enough time. Helical nano-sculptured thin film on glass substrates were deposited ($18 \times 18 \text{ mm}^2$ microscope slide) using electron beams in Edwards system (Edward E19 A3) with a base pressure of 2×10^{-8} torr and a deposition rate of 1 \AA s^{-1} at room temperature. The purity of Manganese was $>99.98\%$ and the deposition angle (α°) was fixed at 80° . In order to achieve a uniform deposition on the substrates, a 30 cm distance was chosen between the evaporation source and the substrate and we expected that vapour has a straight trajectories (i.e., without scattering due to the large mean free path $\sim 10^3\text{-}10^4 \text{ cm}$ [24]). Fig1 shows the schematic diagram of the evaporation system associated with the ability substrate rotation for nano-sculptured chiral thin films growth. The substrates were fixed on the substrate holder, which was connected to a computer by stepper motor, with 10cm diameter from stainless steel. The substrate holder whose rotation is controlled by previously-written and installed software is rotated about its surface normal with rotation speed of 0.0092rpm during the process of deposition [25]. In this regard, the deposition rate was measured by a quartz crystal deposition rate controller (SQM-160-USA, sigma) that was put close to the substrate and at the same azimuthal angle of substrate. The production of the above-mentioned samples took place by the deposition of Mn on the fixed substrate for a pre-set time with the said deposition rate and then the substrate was rotated continuously until the helical nanostructure with the required thickness was procured. It should not be left unmentioned that the pitch of nanostructure is consistent with the deposition time and deposition rate used [25]. The deposition was carried out with the clockwise rotation of the substrate holder and the helical structures were, therefore, produced with 1 pitch. The diameter of the vertical chirals including the width of rings may be estimated as $\approx 200 \text{ nm}$. It is essential to mention here that we calculated the film

thickness (d) or the pitch of the chiral shapes (2Ω) using the tangent rule $\beta = \alpha - \sin^{-1}\left(\frac{1-\cos(\alpha)}{2}\right)$, $\alpha > 60^\circ$ and relation $2\Omega = \frac{2\pi}{\omega} l \sin(\beta)$ [26]; the thickness of each chiral single ring deposited arranged to be about 400 nm. Furthermore, the surface physical morphology and its roughness were obtained by Atomic Force Microscope (AFM) analysis with a Si tip of 10nm radius in noncontact mode. And last but not east, transmission and reflection spectra of Manganese chiral single ring nano-structure were measured in the wavelength region of 300-2500nm at normal incidence angle using single beam spectrophotometer with 2nm wavelength steps.

To compute the optical constants such as the refractive index (n) and the absorption index (k) of the thin films on the glass transparent substrate at different wavelength, we applied the transmittance and reflectance spectra. As it mentioned about the thin film before, it is the deposited chiral single ring on the glass substrate if the film thickness d and a complex refractive index is given $\hat{n} = n - ik$. The extinction index $\alpha(\lambda)$ is procured from the experimental measurements of the transmittance $T(\lambda)$ and reflectance $R(\lambda)$ and the film thickness d according to the following equation [27]:

$$\alpha = \frac{1}{d} \ln \left[\frac{1-R^2}{2T} + \sqrt{\frac{1-R}{4T^2} + R^2} \right] \quad (1)$$

The absorption index k as a function of the wavelength is obtained according to the following equation:

$$k = \frac{\alpha\lambda}{4\pi} \quad (2)$$

Therefore, the refractive index n as a function of the reflectance $R(\lambda)$ and the absorption index $k(\lambda)$ is calculated by the Fresnel formula as [28]:

$$n = \left(\frac{1+R}{1-R} \right) + \sqrt{\frac{4R}{(1-R)^2} - k^2} \quad (3)$$

The optical constants n and k were estimated by giving serious consideration to the experimental errors in measuring $T(\lambda)$ and $R(\lambda)$ as $\pm 2\%$.

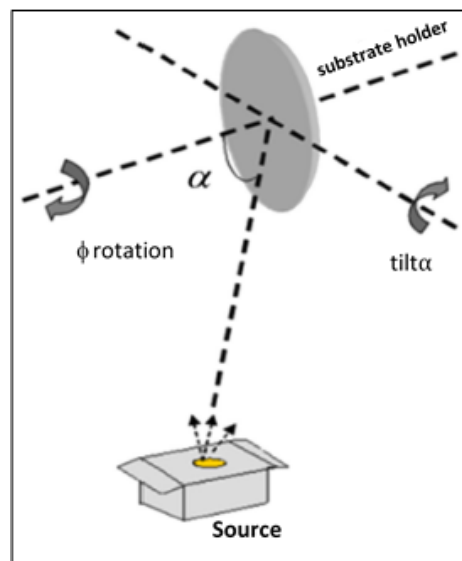


Fig. 1: The schematic of oblique angle deposition in conjunction with rotation of substrate holder

3. Results and Discussion

In Fig 2, 2D, 3D AFM and the surface void images of Manganese chiral single ring are given in columns a, b and c respectively. The results which we obtained from the 3D AFM images that enabled us to observe the unevenness of the surface are as follows: the size of the grains on the film surface, the surface roughness (unevenness) and the surface void fraction. In addition, it is true to say that the surface of the thin film tends to be rough due to the high diffusion effect and the arriving higher vapour flux. RMS and mean surface roughness of the substrates were measured by AFM and were 5.84 nm and 4.6 nm respectively; diameter of the grains and the surface roughness of the films were measured using the J- Microvision software. We can also obtain the surface void fraction (f_v) using the AFM measurements and a simple program in Matlab software (i.e., white color_regions in Fig. 2c). This shows that the films prepared with the GLAD methods are the porous films. The quantitative data obtained from the AFM images are given in Table 1.

Table 1: The structural parameters a Mn chiral single ring film

Diameter of the grains (nm)	Surface void fraction (f_v) (%)	Surface roughness (RMS)	Surface roughness (AVG)
83.33	26.50	5.84	4.6

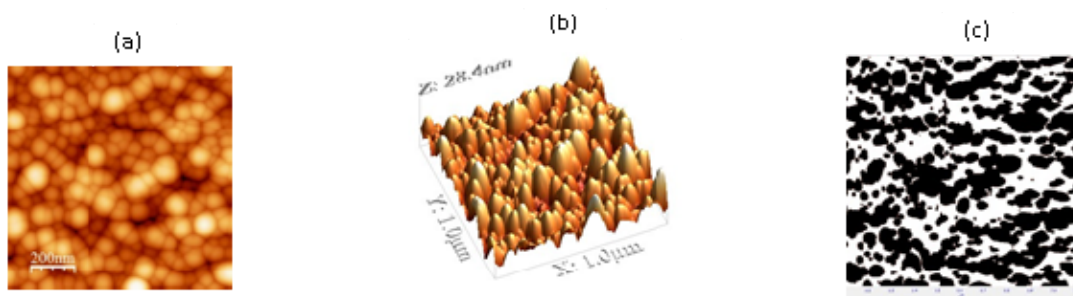


Fig. 2: a) 2D and b) 3D AFM images and c) the surface void image of Manganese chiral single ring

Fig. 3 Shows the schematic diagram of a Mn chiral single ring nanostructure. The helical radius R is fixed to be 100 nm and the pitch height is 2Ω . The incident directions are along helical axis, as shown in Fig3. Optical spectra of the Manganese chiral single ring thin film were measured in the wavelength region of 300 to 2500 nm and are given in Figures 4 and 5. Both reflectance and transmittance spectra were measured at the normal incident light.

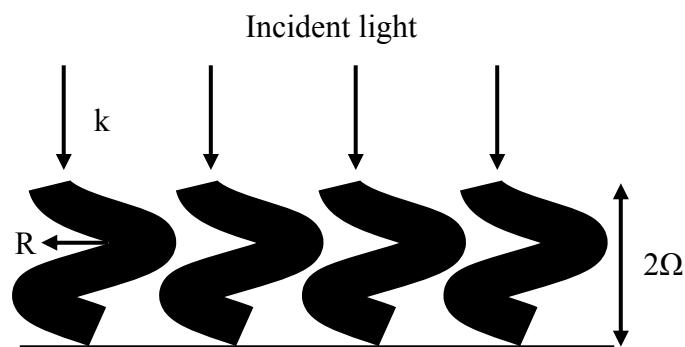


Fig. 3: The schematic for the chiral single ring and the incident light direction

Table 2 displays the details of both intensity and absorption and reflection peak positions for chiral single ring sample. Given the AFM results, to get the optical measurements such as the experimental absorption, transmittance and reflectance, the following parameters were taken into account:

- (1) In case of particles whose size is smaller than the wavelength of the incident light, the electromagnetic wave cannot distinguish their structural details, moreover, the small size of particles can be neglected from the scattering contribution. Therefore, regarding the reflection (R) and transmittance (T) spectra, the absorption spectra can be obtained by using the formula $(1-R-T)$. It is to say that the particle size is 83.33 nm in our project, which is smaller than the minimum wavelength of the incident light (i.e., 300 nm).
- (2) The factors such as the void fraction, surface roughness, the size of grains, and the film thickness are affected by the reflection and absorption spectrum. As it was already shown by several authors [29-31], a smaller grains size, the void fraction, and roughness lead to a rise in reflection. When the size of grains becomes smaller, the density of layer increases and as a result, the void fraction and surface roughness reduces and the surface becomes smoother that results in a rise in the reflection. While the diameter of grains and the fraction of surface void in our work are 83.33 nm and 26.5% alternatively and the RMS and AVG surface roughness are 5.84 nm and 4.6 nm alternatively (Table 1), the reflection increases (around 30%). The reflectance spectra in Fig. 4a show the peaks in UV and visible wavelengths regions. These peaks which are given in Table 2 are about 327, 449, and 880 nm. Fig. 4b shows the wavelength dependence transmittance of nanostructure of Mn chiral single ring. In this regard, Savaloni et al. [32] produce Mn helical structures with square, rectangle and pentagon shapes and showed that the transmittance will considerably increase when wavelengths are larger than the film thickness. It should be noted that the film thickness is about 400nm in this project. Therefore, the transmittance increases as we increase the wavelength, on the other hand, the transmittance spectra becomes constant almost in $\lambda > 1500$ nm and does not depend on the wavelength.

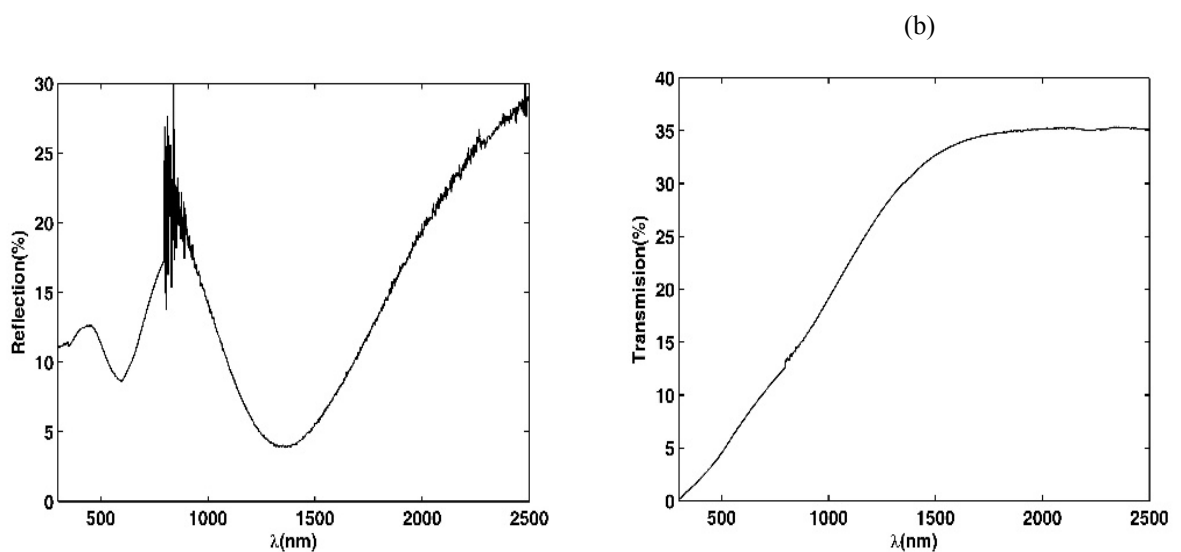


Fig.4: a) Reflection and b) Transmission spectra of Manganese chiral single ring thin film

Table 2: The details of both intensity and absorption and reflection peak positions for nano-structure of Mn chiral single ring

	Wavelength (nm)			Intensity (%)		
Reflection	327	449	880	11.21	12.61	18.61
Absorption	300	555	1188	88.77	84.41	68.06

(3) Fig. 5 shows the absorption spectra of Mn chiral single ring nanostructure. We may clearly observe two peaks, one at the lower wavelengths (i.e, 555 nm) and the other at the longer wavelengths (i.e, 1188 nm). In addition, one distinguishing the peak at the lower wavelength has the higher intensity of the absorption (Table 2). Siabi and Savaloni [33] showed that the optical response of metallic structures that is affected by a limited thickness has no effect on the optical spectra (~320 nm). Therefore, it may be suggested that the optical results discussed in this paper are related to the top 320nm thickness of the film. Hence, considering that the thickness of film in this work is about 400 nm, the light may interact with a complete pitch at the low wavelength. However, when the wavelength increases, the light may not interact with sections of the underlying pitch and may only interact with the top surface of the film. This will decrease the intensity of the absorption spectra. In other words, when the wavelength goes up, the number of particles interacting with the light goes down. It can be observed that the peak at long wavelength has the lower intensity of the absorption.

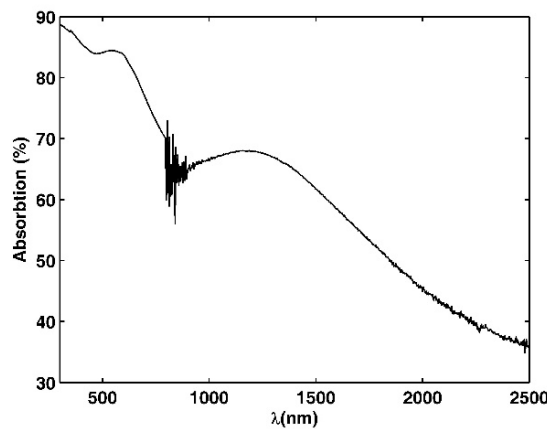


Fig.5: Absorption spectra of Manganese chiral single ring thin film

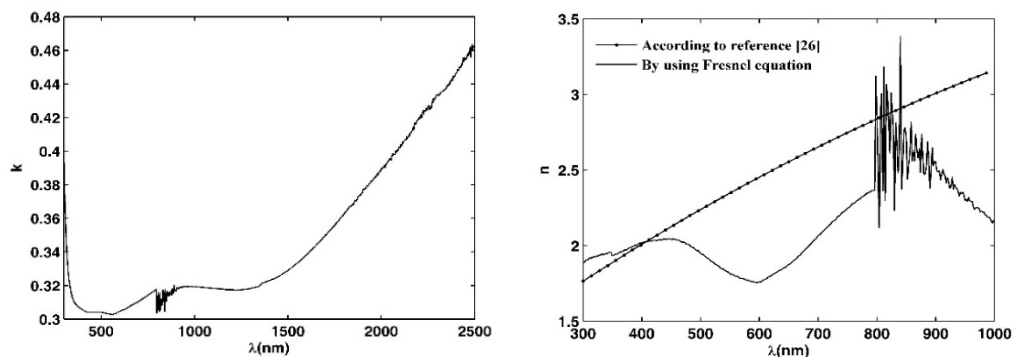
(4) Considered as a function of wavelength, the refractive index (n) and the absorption index (k) of Manganese chiral single ring were attained from the experimental results at normal incident light through using the equations (1) to (3) as it was shown in Fig. 6.

Fig. 6a illustrates a plot of k versus wavelength for nano-structure of Manganese chiral single ring. As a function of wavelength, the plot of k changes exponentially while the absorption index does not change significantly in the visible wavelengths region. It should be noted here that the absorption index increases extensively at very long wavelengths.

Wang and et al., prepared nanostructure TiO₂ [34] and ZnS [35] thin films by employing angle deposition technique and show that the packing density of films decreases as the incident angle increases. At the flux angle of $\alpha=80^\circ$ and 75° , the packing density and the refractive index decrease. It can be attributed to the porous structure in GLAD films, which will inevitably result in the decrease of the effective refractive index.

In the present paper, the results obtained from the refractive index n of nano-structure of Manganese chiral single ring was compared with the structure of Manganese thin film according to reference [36]. Fig. 6b shows the refractive index n of Manganese thin film and Manganese chiral single ring nano-structure as a function of wavelength in the UV and visible regions of 300 to 1000 nm. The peaks can be observed at about 440 and 860 nm in the optical constant n due to the rise in reflectance of the film in which the refractive indices are 2.043 and 2.560 respectively (Fig. 6b). While indices of Manganese thin film, according to reference [37], are obtained $n= 2.102$ and 2.941 at the wavelengths 440 and 860 nm respectively. In this work, we report that Manganese chiral single ring nano-structure prepared by GLAD method is the porous structure and its refractive index is lower than that of the thin film at most of the wavelengths. In particular, at the wavelength of 590 nm, the refractive index extensively reduced to 1.345 (Fig. 6b), which is even less than that of Manganese thin film. Hence, the refractive index of the porous nano-structure depends on the wavelength. Therefore, using density and porous of thin film, the GLAD technique can control the refractive index of the nano-structure.

Fig. 6: Plot of optical indices of Manganese chiral single ring thin film a) Absorption index and b) Comparison of refractive index n of Manganese thin film according to reference [36] and Manganese chiral single ring nano-structure



4. Conclusions

In this paper, we reported that Manganese chiral single ring nano-structure prepared by GLAD method is the porous nanostructure. The porosity of thin film is affected by the reflection and absorption spectrum. Using the experimental results R , T , and the Fresnel formula, we obtained the optical constants n and k . While the refractive and absorption indices depend on the wavelength, the absorption index k as a function of wavelength changes exponentially. The refractive indices of Manganese chiral single ring are about $n= 2.043$ and 2.560 at the wavelengths of 440 and 860 nm respectively, which are lower than those of the corresponding Manganese thin film because nano-structure of Manganese chiral single ring is the porous nano-structure. Therefore, the GLAD technique can control the refractive index of the nano-structure by density and the porous of thin film.

References

- [1] T. Tran, T. Nguyen; Controlled growth of uniform noble metal nanocrystals: Aqueous-based synthesis and some applications in biomedicine, *Colloids and Surfaces B: Biointerfaces* Vol. **88**, no. 1, pp. 1–22, 2011.
- [2] P. K. Jain, K. S. Lee, I. H. El-Sayed and M. A. El-Sayed; Calculated Absorption and Scattering Properties of Gold Nanoparticles of Different Size, Shape, and Composition: Applications in Biological Imaging and Biomedicine, *J. Phys. Chem. B* **110** (2006) 7238.
- [3] A. Mahapatro; Bio-functional nano-coatings on metallic biomaterials, *Materials Science and Engineering: C*, Vol. **55**, pp. 227–251, 2015.
- [4] Z. Karimi, L. Karimi, H. Shokrollahi; Nano-magnetic particles used in biomedicine: Core and coating materials, *Materials Science and Engineering: C*, Vol. **33**, no. 5, pp. 2465–2475, 2013.
- [5] J. Arul Mary, J. Judith Vijaya, L. John Kennedy, M. Bououdina; Microwave-assisted synthesis, characterization and antibacterial properties of Ce–Cu dual doped ZnO nanostructures, *Optik - International Journal for Light and Electron Optics*, 2015.
- [6] K. Ashtari, J. Fasihi, N. Mollania, K. Khajeh; A biotemplated nickel nanostructure: Synthesis, characterization and antibacterial activity, *Materials Research Bulletin*, Vol. **50**, pp. 348–353, 2014.
- [7] S. Pal, Y. K. Tak and J. M. Song; Does the Antibacterial Activity of Silver Nanoparticles Depend on the Shape of the Nanoparticle? A Study of the Gram-Negative Bacterium *Escherichia coli*, *J. M. Appl. and Env. Mic.* **73** (2007) 1712.
- [8] Tariq Jan, Javed Iqbal, Muhammad Ismail, Noor Badshah, Qaisar Mansoor, Aqsa Arshad, Qazi M. Ahkam; Synthesis, physical properties and antibacterial activity of metal oxides nanostructures, *Materials Science in Semiconductor Processing*, Vol. **21**, pp. 154–160, (2014).
- [9] N. M. Ahmed, Z. Sauli, U. Hashim, Y. Al-Douri; Investigation of the absorption coefficient, refractive index, energy band gap, and film thickness for Al_{0.11}Ga_{0.89}N, Al_{0.03}Ga_{0.97}N, and GaN by optical transmission method, *IJNM*, Vol. **2**, No. 2, (2009), pp. 189 - 195.
- [10] H. Nadir, M. Khudheir, R. Hayfa, M. Hazim; Electric field distribution in weakly absorbing monolayer at oblique incidence of light, *IJNM*, Vol. **6**, No. 2, (2013), pp. 87-95
- [11] Z. Y. Zhang and Y. P. Zhao; Optical properties of helical Ag nanostructures calculated by discrete dipole approximation method, *Appl. Phys. Lett.* **90** (2007) 221501.
- [12] M. Wan, M. Tian, S. Yuan, X. Sun, J. He; Surface plasmon modes of infinite cylindrical metallic nanostructures, *Optik - International Journal for Light and Electron Optics*, Vol. **124**, no. 24, pp. 7036–7039, (2015).
- [13] J. Z. Zhang and C. Noguez; Plasmonic Optical Properties and Applications of Metal Nanostructures, *Plasmonics* **3** (2008) 127.
- [14] Z. Y. Zhang and Y. P. Zhao; Optical properties of helical Ag nanostructures calculated by discrete dipole approximation method, *Appl. Phys. Lett.* **90** (2007) 221501.
- [15] M. Akhlaghi; Optimization of the plasmonic nano-rods-based absorption coefficient using TLBO algorithm, *Optik - International Journal for Light and Electron Optics*, Vol. **126**, no. 24, pp. 5033–5037, (2015).
- [16] Z. Wang, X. Quan, Z. Zhang, P. Cheng; Numerical studies on absorption characteristics of plasmonic metamaterials with an array of nanoshells, *International Communications in Heat and Mass Transfer*, Vol. **68**, pp. 172–177, (2015).

- [17] K. L. Kelly, E. Coronado, L. L. Zhao, G. C. Schatz; The Optical properties of metal nanoparticles: the influence of size, shape, and dielectric environment, *J. Phys. Chem.* **B107**
- [18] N. O. Young and J. Kowal, *Nature (London)* **183**, 104 (1959).
- [19] T. Motohiro and Y. Taga, *Appl. Opt.* **28**, 2466 (1989).
- [20] K. Robbie and M. J. Brett, *J. Vac. Sci. Technol. A* **15**, 1460 (1997).
- [21] A. C. van Popta, J. C. Sit, and M. J. Brett, *Appl. Opt.* **43**, 3632 (2004).
- [22] Z. Y. Zhang and Y. P. Zhao, *Appl. Phys. Lett.* **90**, 221501 (2007).
- [23] Z. Y. Zhang and Y. P. Zhao, *APP. Phy.* **104**, 013517 (2008).
- [24] L. Eckertova, *Physics of Thin Films*, chapter 1, Plenum Press, 2nd edition, (1990).
- [25] H. Savaloni, F. Babaei, S. Song, and F. Placido; Characteristics of sculptured Cu thin films and their optical properties as a function of deposition rate, *App. Sur. Sci.*, vol. **255**, no. 18, pp. 8041–8047, (2009).
- [26] H. Savaloni, *surface Science of Nanotechnology*, Vol.1 , (University of Tehran Press, 2671, (2005)
- [27] M.M. El-Nahass, A.A.M. Farag, A.A. Atta, *Synth. Met.* **159** (2009) 589.
- [28] P.P. Banerjee, *Proc. IEEE* **73** (2005) 1859.
- [29] C. Pecharroman, E. D. Gaspera, A. Martucci, R. E. Galindod, P. Mulvaney, *J. Phy. Chem. C* (2015), **119**, 9450-9459.
- [30] N. D. Singho, N. A. C. Lah, M. R. Johan, R. Ahmad, *IJRET*, Vol. **1**, No. 4, 2012 . [31] O. Carton, J. Ghaymouni, M. Lejeune, A. Zeinert, *Journal of Spectroscopy*, Vol. (2013).
- [32] A. Siabi-Garjan, H. Savaloni, " Extinction spectra and electric near-field distribution of Mn nano-rod based sculptured thin films: experimental and discrete dipole approximation results," *Journal of Optics*, (2013).
- [33] Araz Siabi-Garjan and Hadi Savaloni, "Extinction spectra and electric field enhancement of silver chiral nano-flower shaped nanoparticle; comparison of discrete dipole approximation results with experimental results" *Eur. Phys. J. B* (2013) 86: 257
- [34] S. Wang, G. Xia, H. He, K. YI, J. Shao, Z. Fan, *Alloys and Compounds* **431** (2007) 286-291.
- [35] S. Wang, X. Fu, G. Xia, J. Wang, J. Shao, Z. Fan, *App. Surf. Sci* **252** (2006) 8734-8737.
- [36] E.D. Palik, *Handbook of Optical Constants of Solids* (Academic, New York, 1985)

